ARTICLE

Antimicrobial Activities and Cellular Responses to Natural Silicate Clays and Derivatives Modified by Cationic Alkylamine Salts

Shan-hui Hsu,*,† Hsiang-Jung Tseng,‡ Huey-Shan Hung,§ Ming-Chien Wang,‡ Chiung-Hui Hung,‡ Pei-Ru Li,† and Jiang-Jen Lin*,†,||

Institute of Polymer Science and Engineering, National Taiwan University, Taipei 10617 Taiwan, Republic of China, Department of Chemical Engineering, National Chung Hsing University, Taichung, 40227 Taiwan, Republic of China, Graduate Institute of Basic Medical Science, China Medical University, Taichung, 40402 Taiwan, Republic of China, and Center of Nanoscience and Nanotechnology, National Chung Hsing University, Taichung, 40227 Taiwan, Republic of China

ABSTRACT Nanometer-scale silicate platelet (NSP) materials were previously developed by increasing the interlayer space and exfoliation of layered silicate clays such as montmorillonite and synthetic fluorinated mica by the process of polyamine exfoliation. In this study, the antibacterial activity and cytotoxicity of these nanometer-scale silicate clays were evaluated. The derivatives of NSP (NSP-S) which were modified by C18-fatty amine salts via ionic exchange association exhibited the highest antibacterial activity in the aqueous state among all clays. The high antibacterial activity, however, was accompanied by elevated cytotoxicity. The variations of cell surface markers (CD29 and CD44) and type I collagen expression of fibroblasts treated with the clays were measured to clarify the mechanism of the silicate-induced cytotoxicity. The signal transduction pathway involved the downregulation of extracellular-signal-regulated kinase (ERK), which appeared to participate in silicate-induced cytotoxicity. This study helped to understand the antibacterial potential of NSP and the interaction of natural and modified clays with cellular activities.

KEYWORDS: montmorillonite • mica • silicate platelet • cytotoxicity • extracellular-signal-regulated kinase (ERK)

1. INTRODUCTION

Natural clays such as montmorillonite (MMT) and mica have been known as natural medicine for thousands of years. It is generally believed that the clays possess healing functions for internal detoxifying (e.g., the digestive system and liver), trauma injuries, skin conditions, and so on. The therapeutic functions of clays may be associated with their nanosheet structure and ionic charge association. Studies have shown that the layered clays may be intercalated with cetylpyridinium cationic organics in the clay gallery, and these species have been found to be effective for adsorbing microorganisms (1). More recently, the intrinsic antibacterial properties of iron-rich clay minerals have been demonstrated (2).

One of the common smectite clays, MMT, consists of two hydrated aluminosilicates with Si−O tetrahedra and sandwiched Al−O(OH)$_2$ octahedra, with a neighboring plate distance of 12 Å. The clay materials and their multiple interlayer spaces have been reported to serve as a container for encapsulating organic drugs or DNA and have been proposed for use in cancer treatment or gene therapy (3−5). Recently, research efforts have been directed to the uses of nanosized silicate clays for antibacterial purposes and interacting with biomolecules (6). Previously, the common MMT and the synthetic fluorinated mica (Mica) clays were spatially enlarged by incorporating the polyether-amine salts and subsequently embedding with large biomaterials such as bovine serum albumin (BSA) (7, 8). The process indicated the possibility of using the silicate clays for encapsulating protein in the layered structure. In addition to the interaction with protein, the aluminosilicates have been assessed for their cytotoxicity (9, 10). However, there is a lack of studies of specific cellular response or signal transduction.

Anionic clays have attracted increasing interest as nanovehicles for delivering genes, drugs, and bioactive molecules into cells. Smectite clays are suggested to be good delivery carriers of hydrophilic drugs. They are expected to enhance the encapsulation efficiency of drugs. In one study, the clay was shown to reduce the adverse effect of donepezil because the clay used was able to reduce the acidity by absorbing proton and to control the drug release behavior (11). It was also thought that by optimizing the level of the organosilicate additive to the polymer matrix, superior control over drug release kinetics and simultaneous improvements in adhesive properties could be attained for a transdermal pressure-sensitive adhesive formulation (12).

* To whom correspondence should be addressed. E-mail: jianglin@ntu.edu.tw (J.-J.L.); shhsu@ntu.edu.tw (S.-h.H.).
Received for review July 18, 2009 and accepted October 22, 2009
† National Taiwan University.
‡ Department of Chemical Engineering, National Chung Hsing University.
§ China Medical University.
|| Center of Nanoscience and Nanotechnology, National Chung Hsing University.
DOI: 10.1021/am900479q

Published on Web 11/10/2009

Recently, we have developed a process of exfoliating the layered silicate clays and isolating the nanometer-sized silicate platelets (NSP, ca. 100 × 100 × 1 nm^3 in dimension) as new forms of silicate materials (13−15). The exfoliation was confirmed by XRD patterns (16). The NSP inorganic silicates can be further modified by various surfactants such as a C18-alkyl quaternary ammonium salt through an ionic exchange reaction (17). In this study, we compared the antimicrobial ability and cytotoxicity of natural clays (MMT, Mica), their respective exfoliated clays (NSP, NMP), and the fatty amine capped NSP (NSP-S). Scanning electron microscopy (SEM) was used to visualize the interaction of these clays with bacteria or cells. In addition, the expression levels of several surface markers for connective tissue cells such as CD29 and CD44 were examined to elucidate the possible cellular changes caused by the natural clays and their derivatives. CD29 (integrin β1) is involved in cell attachment, migration, differentiation, and survival by mediating the signal stimuli from the extracellular matrix to the intracellular cytoskeleton (18). Fibronectin, collagen, and laminin are among the ligands that integrin can bind. CD44 is a cell surface glycoprotein which is crucial for cell−cell interactions, cell adhesion, and migration (19, 20). An initial understanding of the fundamental size compatibility and interacting behavior between the nanosized silicate platelet and cell surface is important for future developments of new antimicrobial and drug-delivering nanomaterials.

2. MATERIALS AND METHODS

2.1. Clays. MMT, supplied by Nanocor Co., is the sodium form of smectite silicate clay with a cationic exchange capacity of 120 mequiv/100 g. Mica obtained from CO-OP Chemical Co. (Japan), with the trade name SOMASIFTM ME-100, was a synthetic fluorinated mica of layered silicate clay with a chemical composition of Si (26.5 wt %), Mg (15.6 wt %), Al (0.2 wt %), Na (4.1 wt %), Fe (0.1 wt %), and F (8.8 wt %) and a cation exchange capacity of 120 mequiv/100 g. The exfoliated MMT and Mica, as an NSP and NMP slurry in water, were synthesized according to the procedures described in the literature (14, 15, 21). NSP (the exfoliated MMT) could be further modified by capping with a C18-fatty amine surfactant. The C18-fatty amine modified NSP was abbreviated as NSP-S and was prepared using the *n*-octadecanylamine hydrochloride salt (n-$C_{18}H_{37}NH_3^+$) that anchored on the surface of NSP ($\equiv SiO^-Na^+$) to become an organic platelet complex. The preparative procedure is described below. A water slurry of 10 wt % NSP in water suspension (30 g) was added to 10 wt % n-$C_{18}H_{37}NH_3^+$ in water suspension (70 g) in a round-bottomed flask equipped with a magnetic stirrer. The reactants were heated to 80 °C for 1 h. Because the interaction between NSP and fatty amine was strong, the percentage of NSP complexed with the fatty amine (the efficiency of cappying) was over 99% after 1 h of treatment (22).

The individual sizes of NSP, NMP, MMT, and Mica are about 100 × 100 × 1, 300 × 300 × 1, 100 × 100 × (8−10), and (300−1000) × (300−1000) × (4−6) nm, respectively, confirmed by atomic force microscopy and transmission electron microscopy (14, 21). The size of NSP-S is slightly larger than that of NSP because of the additional size of the C18-fatty amine.

2.2. Cell Culture. Human gingival fibroblasts (HGFs) and bovine endothelial cells (BECs) were used for cell study. HGFs were harvested from healthy gingival tissues obtained during surgical procedures with the adequate informed consent (23). Gingival tissues were cut into small pieces by a surgical knife. BECs were harvested from the bovine carotid artery with the collagenase method (24). Both cells were cultured in Dulbecco's modified Eagle's medium supplemented with 10% fetal bovine serum, 100 units/mL of penicillin, and 100 μg/mL of streptomycin. When the cells grew into confluence, they were passaged at a ratio of 1:3. Cell passages from 3 to 15 were used in this study.

2.3. Bacteria Growth Inhibition Assay. Antibacterial activities were evaluated by two methods, the measurement of the size of the inhibition circle and the counting of colony number after coincubation with clays. The two evaluation methods are described below. For each method, two bacterial strains were used to evaluate the antibacterial activities. These included *Staphylococcus aureus* (*S. aureus*) (BCRC 10451) and *Escherichia coli* (*E. coli)* (BCRC 51540), both purchased from the Bioresource Collection and Research Center; two bacterial strains were used to evaluate the antibacterial activities.

2.3.1. *Inhibition Circle.* The bacterial solution was adjusted to 1.5 × 10^7 CFU/mL, and 100 μL was evenly plated on an agar plate. The solutions of clays (1 wt %, 100 μL) were absorbed onto a filter paper (10 mm diameter, Toyo Roshi Kaisha, Ltd., Japan) which was then placed on the center of the agar plate. After 24 h, the filter paper was removed and the diameter (D) of the clear zone was measured. The size of the inhibition ring was represented as (D − 10)/2 in mm. Double-deionized water (DDW) was used as the control. The procedure was performed under a microscope. The size of the inhibition zone was measured three times and averaged. For each clay (and control), six samples were used to obtain the statistics.

2.3.2. *Direct Coincubation with Clays.* The antimicrobial activities were assessed according to the standard of American Society for Testing and Materials E 2315-03. Bacteria were grown in liquid broth containing beef extract (3 g), peptone (10 g), and sodium chloride (5 g) in 1 L of water. They were cultured in a logarithmic phase of growth prior to adjustment and exposure to the various particles. The bacterial solution was first adjusted to 1.5 × 10^6 CFU/mL by Butterfield's buffered phosphate diluted bacterial broth. Different clays were first adjusted to 1000 ppm, and a 1 mL portion was added to 100 mL of the bacterial solution (i.e., 10 ppm final concentration for different clays). The mixed bacterial solutions were incubated at 35 °C and shaken at a speed of 110 rpm for 0 (immediately), 0.5, 1, 2, 3, 6, 12, or 24 h. At the indicated time point, the bacterial solutions were cooled on ice immediately and diluted serially to the proper concentration for colony counting. A 1 mL aliquot was mixed with agar on each agar plate. After 24 h, the colony numbers were counted to evaluate the antibacterial ability of the clays. DDW containing no clay was used as the control (i.e., 1 mL of DDW was added to 100 mL of the bacterial solution).

2.4. Clay−Bacteria or Clay−Cell Interaction by Scanning Electron Microscopy (SEM). An *S. aureus* or *E. coli* suspension was adjusted to 1.5 × 10^6 CFU/mL, and the final concentration of NSP-S was 10 ppm. A 1 mL portion of the bacterial suspension was transferred to 24 well plates with a 1.5 cm round coverslip glass (Matsunami, Japan) in each well. In the control well, a 1.5 × 10^6 CFU bacterial solution was added. The bacterial broth was removed at 0, 0.5, 1, 2, 3, 6, 12, and 24 h periodically. Bacteria left on the glass were fixed with 2.5% paraformaldehyde at room temperature for $^1/_2$ h at 4 °C overnight. The fixed samples were then dehydrated with alcohol followed by field-emission (FE) SEM (JSM-7401F, JEOL, Japan) observation. In another experiment, HGF were seeded on the coverslip glass in a 24-well plate for 24 h, and then the culture media were replaced with fresh media containing 10 ppm of different clays. After 24 h of incubation, cells were fixed and dehydrated for FE-SEM observation. The FE-SEM images were captured from one location out of at least three similar

locations in a microscopic field after observing at least five fields on the sample surface. These images were considered representative.

2.5. Cytotoxicity Assay. A total of 2×10^4 cells (HGF or BEC) were seeded in each well of a 24-well plate. After being treated with 10 ppm of various clays, cells were harvested for MTT assay at 24, 48, and 72 h. 3-(4,5-Dimethylthiazol-2-yl)-3,5-diphenyltetrazolium bromide (MTT) solution (0.5 mg/mL, 1× phosphate buffered saline (PBS)) was added and incubated for 4 h at 37 °C. The supernatant was removed. An aliquot of dimethyl sulfoxide (DMSO) (Tedia, Fairfield, OH) was added to each well and reacted for 10 min to dissolve any resulting formazan crystals. The absorbance was measured at 550 nm with an ELISA reader (F-2500, Hitachi, Japan). DDW containing no clay was used as the control in the cytotoxicity assay and in all the following cell experiments.

2.6. Cell Surface Marker Expression by Flow Cytometry Analysis. After cultivation with clays for 24, 48, and 72 h, HGFs were harvested for the measurement of surface markers CD29 and CD44. The expression level was quantified by a flow cytometer (BD FACS Caliber, BD Bioscience). Cells were collected and washed with cold PBS and suspended in 10 μL of PBS. A 10 μL portion of antihuman CD29 antibody conjugated with phycoerythrin (PE) (PharMingen, San Diego, CA) or antihuman CD44 antibody conjugated with PE (Abcam, Cambridge, MA) was then added and incubated for 30 min at 4 °C in the dark. PBS containing 1% BSA was used to eliminate the nonspecific binding. The fluorescence intensity was quantified by the WinMDI software (Scripps Research Institute, San Diego, CA). Due to a lack of specific antibodies, the surface markers of BEC were not analyzed.

2.7. Collagen Gene Expression by Reverse Transcription Polymerase Chain Reaction (RT-PCR). HGFs were harvested for total RNA extraction after 24 h of incubation with clays. Total RNA was extracted with Trizol reagent (Invitrogen, Carlsbad, CA) according to the manufacturer's instructions. cDNA was synthesized with RevertAid First Strand cDNA Synthesis Kit (MBI Fermentas, St. Leon-Rot, Germany). The cDNA obtained from 1 μg of total RNA was used for PCR by the PCR Master Mix Kit (Applied Biosystems, Foster City, CA). The primer sequence used for human type I collagen was 5′AACCCTGGTGCTGATGGACAG3′ (forward) and 5′GGACGACCAGCTTCACCAGG3′ (reverse) and for human β-actin (internal control) was 5′TCCTGTGGCATCCACGAAACT3′ (forward) and 5′GGAGCAATGATCCTGATCTTC3′ (reverse). The primer sequence used for bovine type I collagen was 5′TGCTGGCCAACTATGCCTCT3′ (forward) and 5′TTGCACAATGCTCTTGATC3′ (reverse) and for bovine GAPDH (internal control) was 5′TCCCTCAAGATTGTCAGCAA3′ (forward) and 5′AGATCCACAACGGATACATT3′ (reverse). The PCR reaction condition included 28 cycles of denaturing at 94 °C for 30 s, annealing at 56 °C for 30 s, and extension at 72 °C for 45 s. The internal controls were used to ensure the uniformity of loading. The semiquantification of collagen-I/β-actin (for HGF) or collagen-I/GAPDH (for BEC) ratios was performed by densitiometric analysis with the LabWork Image Acquisition and Analysis software.

2.8. Protein Expression by Immunoblot Analysis. Proteins were extracted from HGF or BEC in RIPA buffer (Sigma, St. Louis, MO) and analyzed by SDS-polyacrylamide gel electrophoresis. After being transferred onto a polyvinylidene difluoride (PVDF) membrane, antigens were analyzed with specific primary antibodies. Antibodies against ERK and phospho-ERK were purchased from Cell Signaling Technology, Inc. (Beverly, MA). Antihuman type I collagen antibody was purchased from Chemicon International (Temecula, CA), and type I collagen antibody was purchased from Abcam (Cambridge, MA). Antigen−antibody complexes were detected using horseradish peroxide labeled rabbit antimouse IgG and by an enhanced chemiluminescence (ECL) detection system (Pierce, Rockford, IL). The semiquantification of p-ERK/ERK and collagen-I/β-actin ratios was performed by densitometric analysis with the LabWork Image Acquisition and Analysis software.

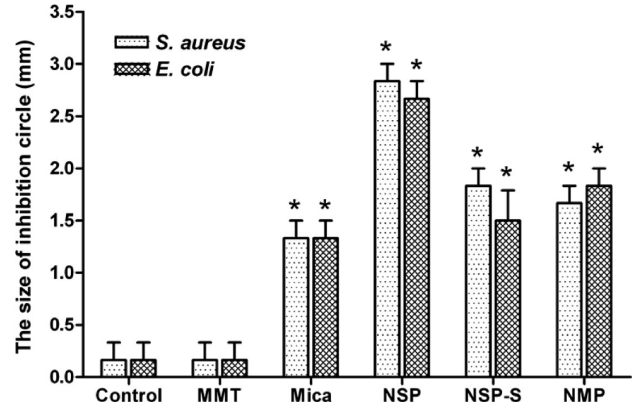

FIGURE 1. Sizes of bacterial inhibition circles for 1 wt % MMT, Mica, NSP, NSP-S, and NMP after 24 h. Asterisks represent statistically significant differences ($p < 0.05$) from the control.

2.9. Statistical Analysis. Except for the measurement of inhibition circle that was performed on six samples, all other experiments were carried out in triplicate. The experiments were repeated to ensure the reproducibility, where data from a typical experiment were shown. Student's t test was used for statistical analyses. Statistical significance was indicated by $p < 0.05$. Data are presented as mean ± standard deviation (SD).

3. RESULTS

3.1. Growth Inhibition Effect against *S. aureus* and *E. coli*. In order to understand the antibacterial property of the clays, the diameter of the bacterial growth circle was measured. The inhibitory effect was examined at concentrations of 10, 100, 1000, and 10 000 ppm. The antibacterial effect as measured by the method of inhibition circle was more evident when the concentration reached 10 000 ppm. The widths of the inhibition circles are shown in Figure 1. NSP had the greatest effect on the inhibition of bacterial growth among all of the clays by this testing method. The pristine MMT clay did not show any inhibitory effect by this method, even at a concentration as high as 10 000 ppm. Both the exfoliated NSP and its derivative modified with C18-alkyl amine salt (i.e., NSP-S) demonstrated significant antimicrobial activity. The relative efficacy is ranked in the following order: NSP > NSP-S ≈ Mica ≈ NMP ≫ MMT.

The antibacterial property of the clays in aqueous suspension at 10 ppm was proven by direct incubation of the clays with *S. aureus* or *E. coli*. The result of colony counts after incubation with time curves for the different clays is shown in Figure 2. For this test, NSP-S showed the most dramatic and notable bacterial inhibition among these silicate clays. The antimicrobial activity was defined at 12 and 24 h. The ranking of antimicrobial activity of the clays appears to be NSP-S > Mica > NSP ≈ NMP ≈ MMT.

The interaction of *S. aureus* or *E. coli* with NSP-S could be visualized by FE-SEM after incubation of the bacteria with NSP-S (10 ppm). The images are presented in Figure 3. As is known, the diameter of *S. aureus* is 0.5−1 μm, the length of *E. coli* is 1.5−2 μm, and the dimension of the nanosheet

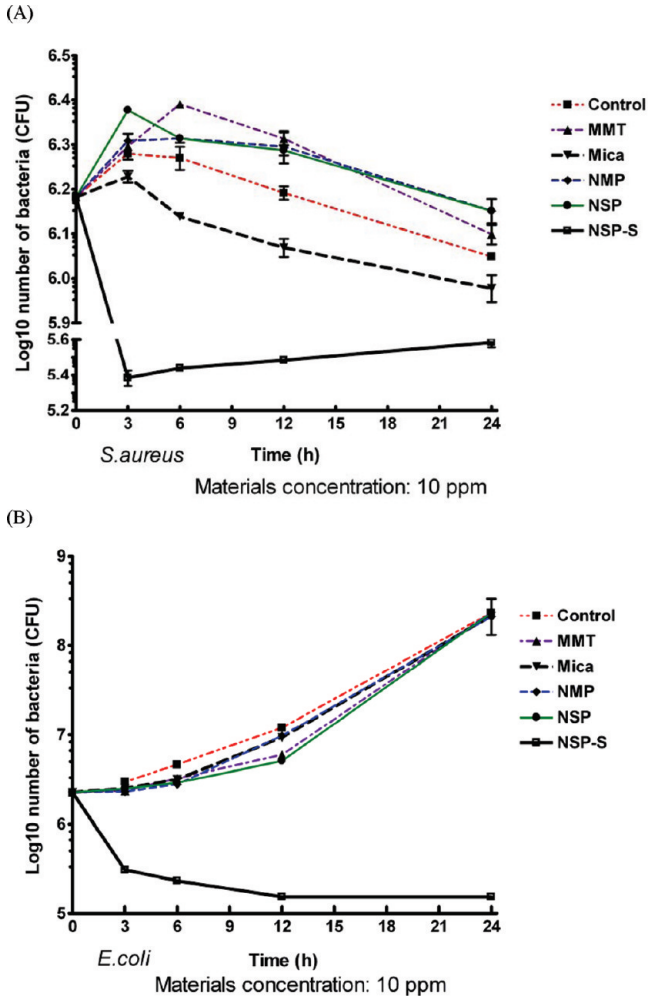

FIGURE 2. Colony numbers of *S. aureus* (A) and *E. coli* (B) after different times of coincubation with MMT, Mica, NSP, NSP-S, or NMP at 10 ppm.

structure for NSP-S is about 100 nm × 100 nm × 1 nm. The images showed that NSP-S covered the surface of the bacteria. As the incubation time increased, some hollow space around the NSP-S was observed (as indicated by the solid black circles in the microscopic images). We suggest that some bacteria may have died and left the hollow space. Some bacteria were still alive (as indicated by the broken-line black circles in the images). The progressive change of the NSP-S—bacteria interaction was accompanied by a decrease in bacterial counts during the incubation with NSP-S.

3.2. Cytotoxicity to HGF and BEC. Figure 4 shows the viability of cells incubated with 10 ppm of the pristine clays (MMT and Mica), the exfoliated platelets (NSP and NMP), and the surfactant-modified NSP-S at 24, 48, and 72 h of incubation period. At 24 h, the viability of HGF in each group was close to the control except in the Mica-treated group (Figure 4A). However, at a time of 48 h, the viability of HGF treated with NSP-S was significantly lower than those treated with other clays. At 72 h, HGF treated with Mica or NSP-S showed a remarkable decrease in viability.

The cytotoxicity of clays on BEC was also evaluated to obtain information on the variance among different cell types. As shown in Figure 3B, BEC treated with 10 ppm of NSP-S had the lowest viability at 24, 48, and 72 h. BEC with MMT had a viability similar to that of the control at 72 h. On the basis of the data in Figure 4B, the trend of cytotoxicity (at 10 ppm) is as follows: NSP-S > Mica > NSP ≈ NMP > MMT.

Due to the size difference between bacteria and cells, the nanosheet structures of clays may interact differently with bacteria from cells. The SEM images (Figure 5) clearly showed the appearance of clays and clay aggregates of various sizes on the cell surface. The sheet dimension of Mica is inherently larger than that of the other clays. The aggregates of the exfoliated NMP were not as obvious as those of the pristine Mica, however, they were more obvious than all of the MMT-derived clays. The particle sizes of MMT, NSP, or NSP-S were smaller than those of Mica or NMP, which could be one reason for the interaction.

3.3. Effects on Expression Levels of Cell Surface Markers. Flow cytometry was used to analyze the change in the levels of CD29 and CD44 proteins on HGF. Figure 6A shows that CD29 on the cell surface was significantly reduced after incubation with clays for 72 h, especially with Mica and NSP-S. Although CD29 seemed to be reduced after incubation with Mica and NSP-S for 48 h, there was no statistical significance found between the control group and any clay at 24 and 48 h. The change in CD44 expression on the surface of HGF treated with clays is demonstrated in Figure 6B. After 48 h, the CD44 expression level was reduced by Mica and NSP-S with statistical significance ($p < 0.05$). The expression profile of CD44 at 72 h was similar to that at 48 h for all groups; i.e. CD44 expression was significantly reduced by Mica and NSP-S ($p < 0.05$).

3.4. Effects on Type I Collagen Expression Level and ERK Phosphorylation. The effect of clays on type I collagen expression in HGF (Figure 7A,B) and BEC (Figure 7A,C) was analyzed by RT-PCR and Western blot analysis. Type I collagen expression was significantly reduced in Mica- and NSP-S-treated groups, in both mRNA and protein levels. In MMT- and NSP-treated groups, only slight reduction was found. No obvious change was found in the NMP-treated group. The type I collagen expression levels were slightly lower for BEC, but the tendency remained for both cells. To clarify if the ERK pathway was involved, the phosphorylated form of ERK protein (p-ERK) was detected by the specific antibody. The reduction of p-ERK was particularly obvious in Mica- and NSP-S-treated groups, while in the NMP-treated group an increase of p-ERK was observed (Figure 7B,C). These findings were consistent with the tendency of changes in type I collagen expression. It was concluded that Mica and NSP-S had a certain extent of cytotoxicity and they decreased the expressions of CD29, CD44, and type I collagen of HGF. These effects may be correlated with the reduction of p-ERK.

Table 1 summarizes the antibacterial activity and the cellular response of the modified clays in comparison with those of their parent clays. Overall, NSP-S had the highest potential for use in antibacterial applications.

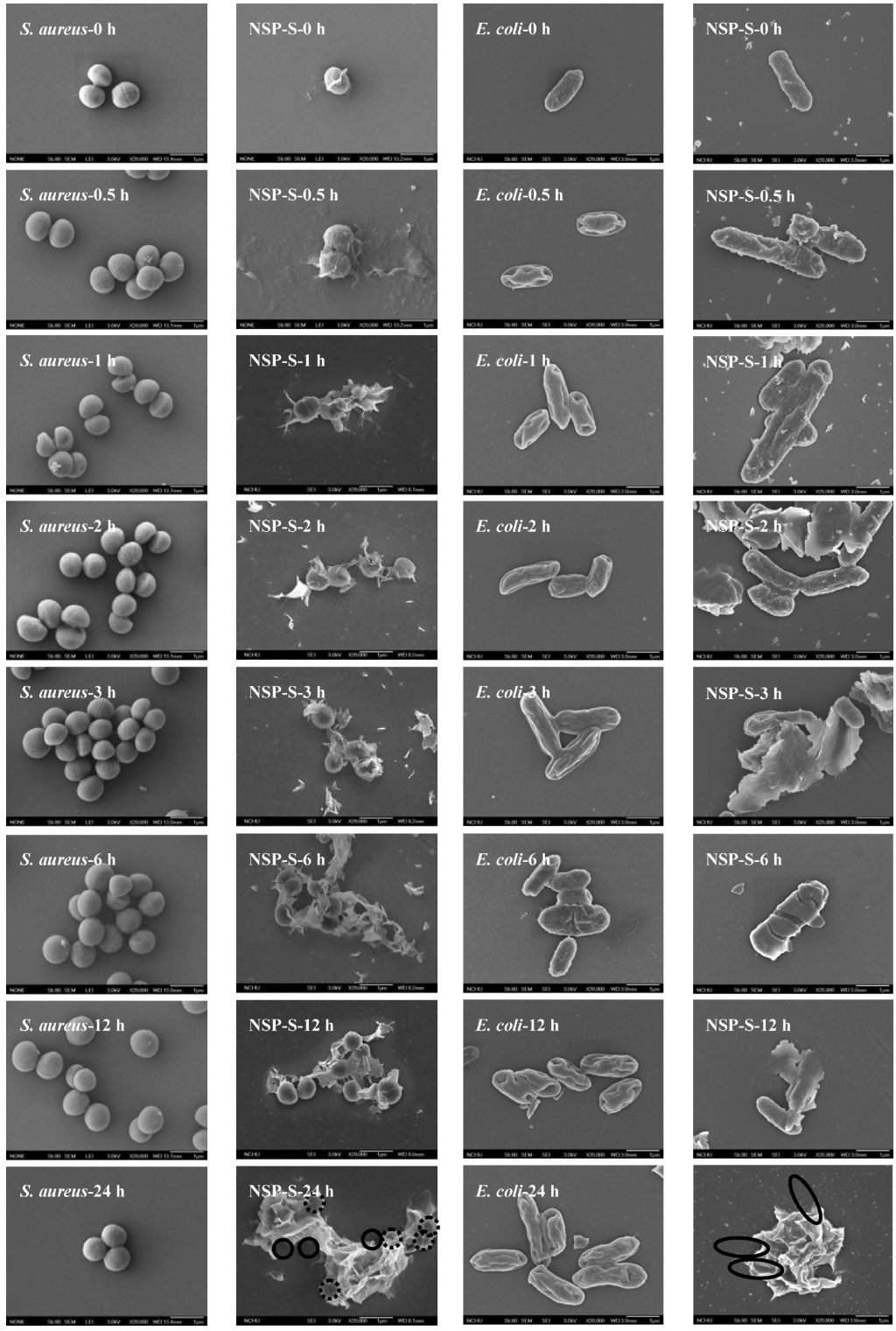

FIGURE 3. FE-SEM images showing the morphology of *S. aureus* and *E. coli* after incubation with NSP-S (10 ppm). The solid black circles show hollow spaces (the space left by the dead bacteria). The broken-line black circles show bacteria that were alive.

4. DISCUSSION

In this study, two different protocols were used to test and compare the antibacterial activities of the parent clays, MMT and Mica, and their exfoliated silicate platelets, NSP, NSP-S, and NMP. In the measurements of inhibition circles, the parent MMT clay failed to show any antibacterial activity toward *S. aureus* and *E. coli*. After exfoliation, NSP gained antibacterial properties. However, the diffusion kinetics in the filter paper and the extent of dispersion of the clays could influence the size of the inhibition circle. If the particles were too large, they might be trapped in the filter paper and difficult to diffuse or spread to effectively contact with the bacteria. For instance, the

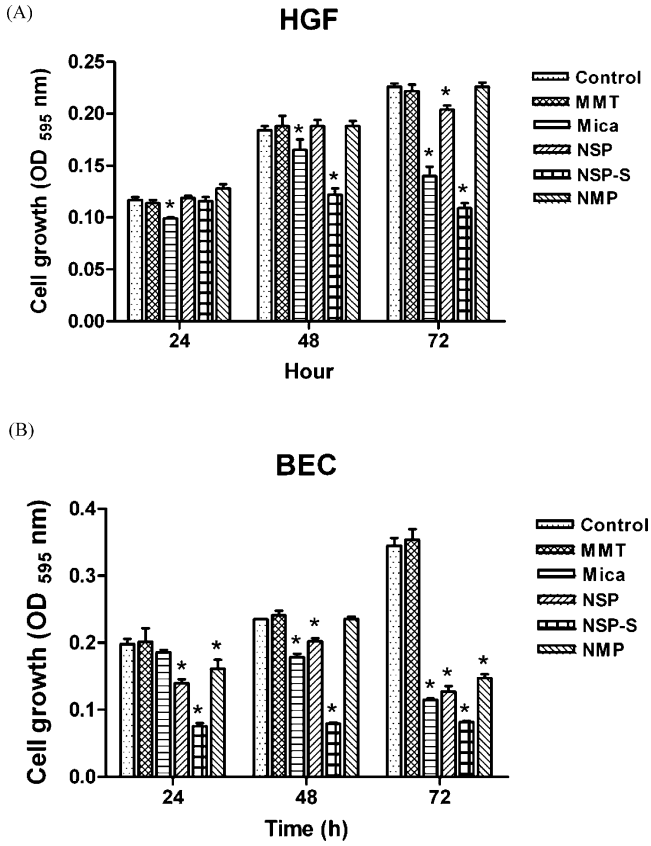

FIGURE 4. MTT assay of HGF (A) and BEC (B) treated with MMT, Mica, NSP, NSP-S, or NMP at 10 ppm. The asterisks represent $p < 0.05$ compared to the control.

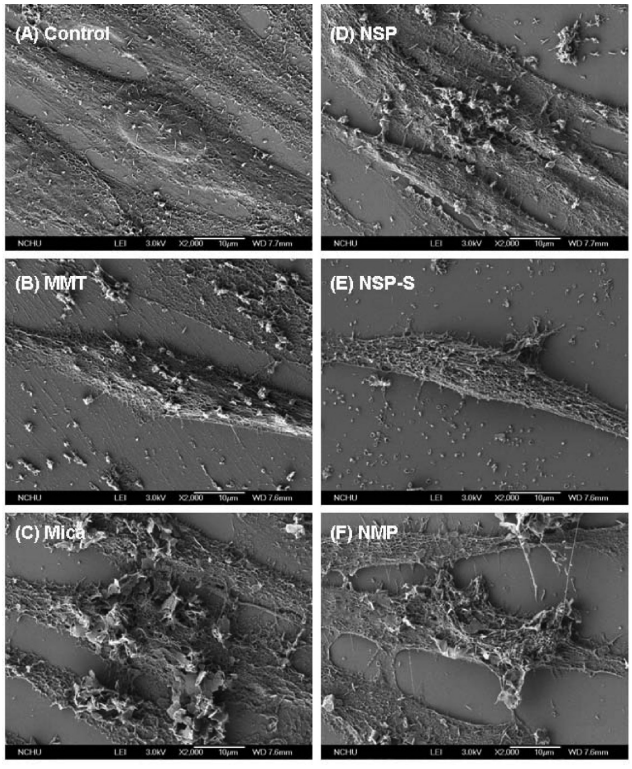

FIGURE 5. FE-SEM images of HGF incubated with 10 ppm of MMT, Mica, NSP, NSP-S, or NMP for 48 h.

inhibition circle was wider for NSP initially (NSP > NSP-S). We believed this was due to the slower diffusion rate of NSP-S.

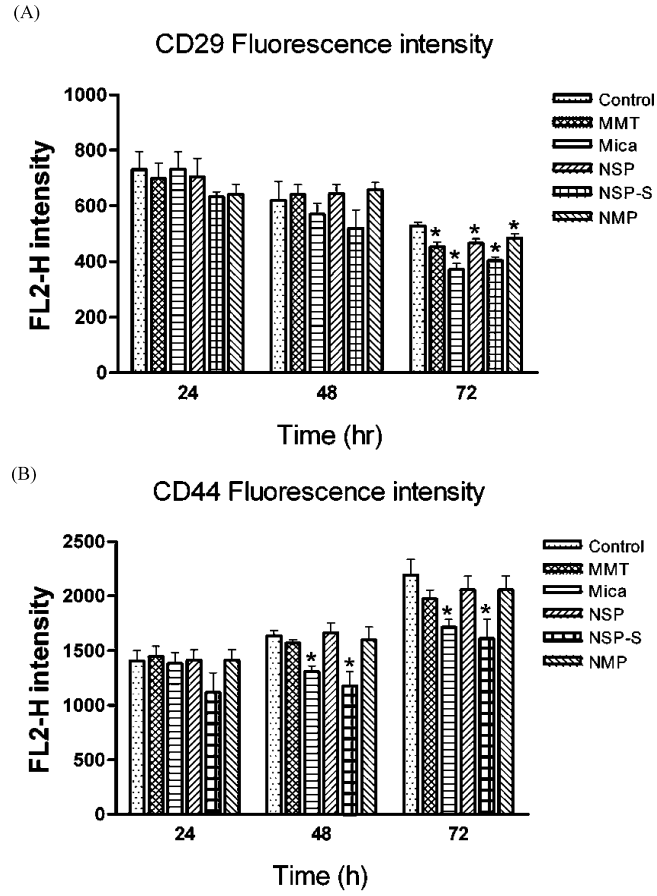

FIGURE 6. CD29 (A) and CD44 (B) expression levels for HGF treated with 10 ppm of MMT, Mica, NSP, NSP-S, and NMP at different time periods. Asterisks represent $p < 0.05$ compared to the control.

Because NSP-S contains C18-fatty amine, NSP-S was larger in size than NSP. The method of inhibition circle involves the diffusion of particles in the filter paper. Therefore, direct incubation may be more appropriate to evaluate the antimicrobial activities of such type of nanomaterials. In the aqueous state, the nanomaterials could express their antibacterial behavior by directly coincubating bacteria with the clays. By the latter method, NSP-S was found to be more effective for inhibiting the bacteria than the other clays examined.

The specific surface areas of NSP, NMP, MMT, and Mica are about 800, 430, 750, and 9 m^2/g, respectively. Therefore, the specific surface area is ranked in the following order: NSP $\approx$ NSP-S > MMT > NMP > Mica. In addition, the difference in platelet size of Mica (300−1000 nm) and MMT (100 nm) may affect the spacing enlargement and surface exposure (15, 16). The zeta potentials of MMT, Mica, NSP and NMP are −18, −60, −5, and −15 mV, respectively, at pH 7.4 (14, 21), and that of NSP-S is +26 mV. This means that these clays are stable in water or in culture medium. However, on contact with cells, aggregation might occur. On the basis of the zeta potential values, NSP-S is more stable than NSP and does not form aggregates easily. This explained why the size of NSP appeared to be larger than that of NSP-S on the cell surface in FE-SEM images.

The efficacy of NSP-S may be explained by the presence of positively charged C18-fatty amine on the surface. The

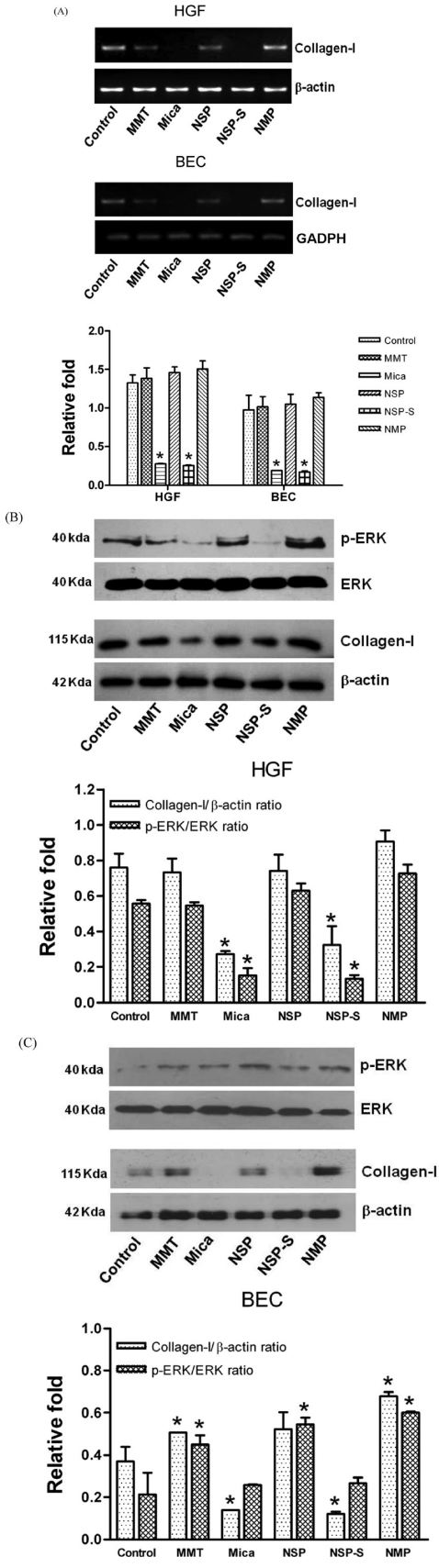

FIGURE 7. Result of type I collagen gene expression for HGF and BEC by RT-PCR (A) and the protein expressions of type I collagen, ERK, and p-ERK by Western blot analysis for HGF (B) and BEC (C). Data are mean ± SD. The asterisks represent $p < 0.05$ compared to the control.

Table 1. Antibacterial Effect and Cellular Response of NSP, NSP-S, and NMP in Comparison with Those of Their Parent Clays[a]

	parent clay/derivative		
	MMT/NSP	MMT/NSP-S	Mica/NMP
antibacterial effect (ASTM E 2315-03) *S. aureus*/*E. coli*	=/=	↑↑↑/↑↑↑	↓/=
cytotoxicity HGF/BEC	↑/↑	↑↑↑/↑↑↑	↓/↓
CD29 (HGF)	=	↓	↑
CD44 (HGF)	=	↓	↑
type I collagen HGF/BEC	=/↑	↓/↓	↑↑/↑↑
p-ERK HGF/BEC	↑/=	↓/↓	↑↑/↑↑

[a] Legend: =, equal or similar; ↑, more (upregulated); ↓, less (downregulated).

zeta potential of NSP-S is +26 mV, as mentioned. The cell wall of bacteria including the Gram positive and negative bacteria was negatively charged. The positively charged NSP-S could bind with the negatively charged bacterial wall. In addition, the capping with C18-fatty amine salts rendered the NSP surface with lipid-like organics which could interact with the bacteria cell wall and were capped on it, as the FE-SEM images suggested. NSP-S fatty amine could interact with the bacterial cell wall as the initial step, causing the dramatic increase in antibacterial activity. The interaction of bacterial wall and fatty amine on NSP-S would make the bacteria accessible and fragile for sustaining the osmotic pressure inside the bacteria. This could rupture the bacteria. The hypothesis involving the chemical structure of NSP-S and interaction through cationic surfactant with the cell wall was further supported by the literature. In the study of Herrera et al. (25), cetylpyridinium (CP) was used as the surfactant to increase the antibacterial activity for the pristine MMT. The surfactant, CP, increased the antibacterial activity of three CP-exchanged clays to a remarkable level, as effective as granulated activated charcoal. The authors suggested that the increased antibacterial activity resulted from the critical surfactant/clay interactions and was not due to the released surfactant. In our study, the bonding between NSP and fatty amine is very strong due to ionic interactions, hydrogen bonds and steric hindrance (22). Additional energy would be required to remove the fatty amine from NSP. The effect of the free surfactant should be minimal.

On comparison of the two pristine clays, MMT did not show a significant inhibition of the growth of *S. aureus* in the aqueous state, but the other parent clay, Mica, decreased the colony count 12% after coincubation for 3 h. The exfoliated NSP-S did decrease the colony number 87% more than NSP, while NMP-S decreased the colony number 66% more than Mica after 24 h of incubation. The two pristine clays did not show a significant result for inhibiting the growth of *E. coli* in the aqueous state, but NSP-S decreased the colony count 99.9% after coincubation for 24 h. These results indicated the increase in surface area by exfoliation could be the key factor contributing to the boosted antimicrobial effect. In addition, the difference in the platelet sizes of Mica (300−1000 nm) and MMT (100 nm) affects the spacing enlargement and surface exposure (15, 16) and

consequently the antibacterial activities. There could be factors other than size differences between bacterial cells and eukaryotic cells that influenced interactions and cytotoxicity NSP. For example, the difference between prokaryotic and eukaryotic cells could be important in cell envelope composition.

The favorable changes in particle size and surface area as a result of exfoliation are important for the antimicrobial effect. On the other hand, particle aggregation could affect the size of the clays and, therefore, the cell−particle interactions. In general, the clays were well dispersed in water and in the culture medium. When the clays were in contact with cells, particle aggregation might have arisen from interaction with the surface of the cells. The aggregation may affect the "covering effect" of the clays and therefore their antimicrobial effect. As mentioned, NSP-S particles are more stable than NSP on the basis of the zeta potential measurement. The modification by C18-fatty amine surfactant causes NSP-S to be better dispersed in the culture medium. This all contributed to the efficacy of NSP-S being better than that of other clays. We believed that the exfoliation and the capping with C18-fatty amine salt were both crucial to the enhanced antibacterial ability of the nanoscale materials. On the other hand, the negatively charged NSP without a surfactant modification showed only a low antibacterial activity compared to NPS-S. The antimicrobial mechanism of NSP is likely to be different from that of Cu(II)-exchanged MMT as reported (1, 26).

By definition, the antimicrobial activities of clays are not bactericidal. Bactericidal activity is defined as a 99.9% reduction of CFU after a specific period of time. The antimicrobial activities of clays were caused by direct contact, sorption, and finally covering of the surface of bacteria. This paper emphasizes the antibacterial but not bactericidal effect of the clay materials. Most bactericidal agents would slaughter cells at the same time, which are not suitable for applications such as biomedical materials.

It is necessary to consider the safety issues if the above clays are used as antimicrobial biomedical materials. Cell viability assays showed that Mica was more toxic to HGF and BEC than MMT. The cytotoxicity of Mica can probably be attributed to the much larger diameter. This large size could prevent cells from taking up enough nutrients from the medium. The growth inhibition effect of NSP-S applied not only to bacteria but also to eukaryotic cells in a similar trend. The eukaryotic cell membrane was also negatively charged and certainly could be sensitive to the positively charged amine groups attached to the silicate layers. We suggest that Mica and NSP-S may have attached to the surface of cells and influenced the surface proteins. Therefore, we investigated the signal transduction pathway related to the cytotoxicity. CD29, the integrin $\beta 1$ subunit and also known as a fibronectin receptor, is highly associated with cell adhesion and migration (18). Integrins are an important family of surface proteins that can receive growth signals from the extracellular matrix. CD44 is another transmembrane protein closely associated with cell−cell and cell−substrate interactions. It plays a crucial role in regulating cell migration and differentiation (19). The interplay of CD44 with its ligands has been reported to modulate adhesiveness, motility, matrix degradation, proliferation, and cell survival (20). The decrease in the expression levels of CD29 and CD44 observed in Mica and NSP-S treated cells could adversely affect the cell attachment and/or interfere with the growth factor binding and eventually may result in cell death. The results of cell surface markers were consistent with the trend in cytotoxicity.

Type I collagen is one of the extracellular matrix components. The gene expression was found to be markedly decreased in Mica- and NSP-S-treated cells. The reduction of type I collagen expression could result in cell detachment. Many factors were reported to regulate the gene expression of type I collagen (27). Especially, it was found that in Mica- and NSP-S-treated groups the phosphorylated ERK was significantly reduced. This finding did not agree with an earlier report (28) which concluded that the activation of the ERK MAPK pathway may downregulate type I collagen gene expression. Signaling pathways may interact with each other and form a network to determine the cell fate. In this study, the expression level of type I collagen and p-ERK were both downregulated when cytotoxicity occurred. Certainly, there are still other signaling pathways related to cell survival such as PI3K/Akt or PKC pathways that can be further investigated. The complicated interaction of these pathways may contribute to the silicate-induced cytotoxicity.

Although a detailed mechanism regarding the interaction of clays with bacteria or cells requires a more in-depth study, the antibacterial effect has been realized by exfoliation and by surface modification. The cytotoxicity was ascribed to the downregulation of cell surface receptors responsible for cell−substrate interaction and to the ERK pathway.

5. CONCLUSION

The silicate platelet materials, especially with surfaces modified by a cationic C18-fatty amine surfactant, were found to have an antibacterial activity. The efficacy is attributed to their nanosize, high surface area, ionic charge interactions, and better dispersion. The results of cytotoxic studies indicated that cytotoxicity was accompanied by the reduced expression of type I collagen and phosphorylated ERK. With the lipid-like fatty amine modification on the silicate platelet surface, the nanometer-sized clays have been proven to be viable for use as antimicrobial agents.

REFERENCES AND NOTES

(1) Herrera, P.; Burghardt, R. C.; Phillips, T. D. *Vet. Microbiol.* **2000**, *74*, 259.
(2) Haydel, S. E.; Remenih, C. M.; Williams, L. B. *J. Antimicrob. Chemother.* **2008**, *61*, 353.
(3) Lin, F. H.; Lee, Y. H.; Jian, C. H.; Wong, J. M.; Shieh, M. J.; Wang, C. Y. *Biomaterials* **2002**, *23*, 1981.
(4) Katti, D. R.; Ghosh, P.; Schmidt, S.; Katti, K. S. *Biomacromolecules* **2005**, *6*, 3276.
(5) Lin, F. H.; Chen, C. H.; Cheng, W. T.; Kuo, T. F. *Biomaterials* **2006**, *27*, 3333.

(6) Podsiadlo, P.; Paternel, S.; Rouillard, J. M.; Zhang, Z.; Lee, J.; Lee, J. W.; Gulari, E.; Kotov, N. A. *Langmuir* **2005**, *21*, 11915.
(7) Lin, J. J.; Wei, J. C.; Juang, T. Y.; Tsai, W. C. *Langmuir* **2007**, *23*, 1995.
(8) Lin, J. J.; Wei, J. C.; Tsai, W. C. *J. Phys. Chem. B* **2007**, *111*, 10275.
(9) Murphy, E. J.; Roberts, E.; Horrocks, L. A. *Neuroscience* **1993**, *55*, 597.
(10) Murphy, E. J.; Roberts, E.; Anderson, D. K.; Horrocks, L. A. *Neuroscience* **1993**, *57*, 483.
(11) Park, J. K.; Choy, Y. B.; Oh, J. M.; Kim, J. Y.; Hwang, S. J.; Choy, J. H. *Int. J. Pharm.* **2008**, *359*, 198.
(12) Shaikh, S.; Birdi, A.; Qutubuddin, S.; Lakatosh, E.; Baskaran, H. *Ann. Biomed. Eng.* **2007**, *35*, 2130.
(13) Chou, C. C.; Lin, J. J. *Macromolecules* **2005**, *38*, 230.
(14) Lin, J. J.; Chu, C. C.; Chiang, M. L.; Tsai, W. C. *J. Phys. Chem. B* **2006**, *110*, 18115.
(15) Chiu, C. W.; Chu, C. C.; Cheng, W. T.; Lin, J. J. *Eur. Polym. J.* **2008**, *44*, 628.
(16) Lin, J. J.; Chen, Y. M. *Langmuir* **2004**, *20*, 4261.
(17) Lin, J. J.; Chu, C. C.; Chiang, M. L.; Tsai, W. C. *Adv. Mater.* **2006**, *18*, 3248.
(18) Brakebusch, C.; Fässler, R. *Cancer Metastasis Rev.* **2005**, *24*, 403.
(19) Mylona, E.; Jones, K. A.; Mills, S. T.; Pavlath, G. K. *J. Cell. Physiol.* **2006**, *209*, 314.
(20) Marhaba, R.; Zöller, M. *J. Mol. Histol.* **2004**, *35*, 211.
(21) Chiu, C. W.; Chu, C. C.; Dai, S. A.; Lin, J. J. *J. Phys. Chem. C* **2008**, *112*, 17940.
(22) Hou, L. T.; Tsai, A. Y.; Liu, C. M.; Feng, F. *Cell. Transplant.* **2003**, *12*, 787.
(23) Hagiwara, H.; Shimonaka, M.; Morisaki, M.; Ikekawa, N.; Inada, Y. *Thromb. Res.* **1984**, *33*, 363.
(24) Hu, C. H.; Xu, Z. R.; Xia, M. S. *Vet. Microbiol.* **2005**, *109*, 83.
(25) Chou, C. C.; Chiang, M. L.; Lin, J. J. *Macromol. Rapid Commun.* **2005**, *26*, 1841.
(26) Tong, G.; Yulong, M.; Peng, G.; Zirong, X. *Vet. Microbiol.* **2005**, *105*, 113.
(27) Ghosh, A. K. *Exp. Biol. Med.* **2002**, *227*, 301.
(28) Chaudhary, L. R.; Avioli, L. V. *J. Cell. Biochem.* **2000**, *76*, 354.

AM900479Q